Quantum spin fluctuations for a distorted incommensurate spiral

Randy S. Fishman

Materials Science and Technology Division, Oak Ridge National Laboratory, Oak Ridge, Tennessee 37831, USA

Quantum spin fluctuations are investigated for the distorted incommensurate spiral state of a geometrically frustrated triangular-lattice antiferromagnet. With increasing easy axis anisotropy, the average reduction of the spin amplitude by quantum fluctuations is suppressed but the spiral also becomes more distorted. Quantum fluctuations enhance both the wave vector of the distorted spiral and the critical anisotropy above which it undergoes a first-order transition into a collinear state. An experimental technique is proposed to isolate the effects of quantum fluctuations from the classical distortion of the spiral. This analysis is applied to the elliptical spiral state of doped $CuFeO_2$.

PACS number(s): 75.10.Hk, 75.30.Kz, 75.50.Ee

I. INTRODUCTION

Spin fluctuations may be either thermal or quantum mechanical in origin. At zero temperature, thermal fluctuations are absent but quantum fluctuations (QFs) can significantly suppress or even prevent magnetic ordering, especially in lower dimensions. While QFs have rather simple effects on the collinear spin states of conventional antiferromagnets (AFs),[1] their effects on noncollinear spins are rather more complex. The effects of QFs on the spin amplitudes and angles of a noncollinear state were recently described[2] for the three-sublattice (SL) state of $CuCrO_2$.[3] Although there have been many studies on the effects of QFs for incommensurate spin spirals with equivalent spins,[4] comparatively little is known about the effects of QFs for incommensurate spirals with inequivalent spins, such as in the presence of anisotropy or a magnetic field. This paper examines the effects of QFs for the incommensurate spiral states of a triangular lattice AF with perpendicular, easy axis anisotropy.

The effects of QFs on incommensurate spirals are important for a wide variety of physical systems. Materials that exhibit incommensurate spiral order include rare earths,[5] manganites,[6] and other several other classes of oxides.[7] We focus on the incommensurate spiral observed in doped $CuFeO_2$.[8] As for the other oxides listed above, the incommensurate spiral state of doped $CuFeO_2$ displays multiferroic behavior with a spontaneous electric polarization produced by the chiral magnetic order.[9]

Of particular interest is understanding how QFs affect the ellipticity of an incommensurate spiral. While the ellipticity of a pure spiral is 1 and the ellipticity of a collinear state is 0, the measured ellipticity of the distorted spiral in multiferroic $CuFeO_2$ is about 0.9.[10] Although the ellipticity contains both classical and quantum contributions, it may be possible to isolate quantum effects from the classical distortion of the spiral, as described below.

Due to the numerical challenge of evaluating QFs in a large unit cell, we shall study QFs for an incommensurate spiral in two dimensions. Because the AF interactions between neighboring planes in $CuFeO_2$ are not geometrically frustrated, a two-dimensional model has provided qualitatively accurate results for the spin state[11] and magnetic phase diagram[12] of $CuFeO_2$. Considering the relative effects of QFs on square and cubic lattices,[1] we expect that the reduction of the

spin amplitudes at $T = 0$ is about 2.5 times larger in two dimensions than in three dimensions for zero anisotropy. But the quantitative predictions of this paper for $CuFeO_2$ should improve with increasing anisotropy, which regulates the momentum integrals by eliminating one of the Goldstone modes. Of course, the qualitative results of this work are also relevant to three dimensions.

A common misconception is that QFs have a negligible effect on the spin amplitudes of materials like $CuFeO_2$ with $S = 5/2$. While it is true that the *relative* reduction of the spin amplitude $\Delta M(\mathbf{R})/S \sim 1/S$ due to QFs is smaller for systems with large spin, the *absolute* reduction $\Delta M(\mathbf{R}) \sim 1$ is, to lowest order in $1/S$, independent of S. By contrast, the rotation of the spin angle $\Delta\theta(\mathbf{R})$ is of order $1/S$. Consequently, QFs induce a greater spin reorientation for noncollinear states with smaller spins. Although the calculations described below were motivated by observations for $CuFeO_2$, the results can be readily extended to treat other spiral states with any spin S.

This paper is divided into five sections. The model for a geometrically frustrated triangular lattice AF with easy axis anisotropy is described in Sec. II. Results of that model for the effects of QFs on the spin amplitudes and angles are presented in Sec. III. Section IV discusses the effects of QFs on the spiral parameters. Section V contains a conclusion.

II. MODEL

As sketched in Fig. 1(a), each hexagonal plane can be described as a triangular lattice with nearest-neighbor AF exchange interactions $J_1 < 0$ and second- and third-neighbor interactions J_2 and J_3. The Hamiltonian of a triangular-lattice AF in zero field is

$$H = -\frac{1}{2}\sum_{i\neq j} J_{ij}\mathbf{S}_i \cdot \mathbf{S}_j - D\sum_i S_{iz}^2, \qquad (1)$$

where $\mathbf{S}_i \equiv \mathbf{S}(\mathbf{R}_i)$ are quantum spins and $D > 0$ is the easy axis anisotropy.

To model $CuFeO_2$, we shall take $S = 5/2$, $J_2 = -0.44|J_1|$, and $J_3 = -0.57|J_1|$.[13] Anisotropy then favors the 4-SL $\uparrow\uparrow\downarrow\downarrow$ state sketched in Fig. 1(b) with spins aligned along the z axis. Taking the hexagonal lattice constant equal to 1, this state has wave vector $\mathbf{Q}_{4\text{-}SL} = \pi\mathbf{x}$. The $\uparrow\uparrow\downarrow\downarrow$ state was first observed in pure $CuFeO_2$ about 20 years ago by Mitsuda *et al.*[14]
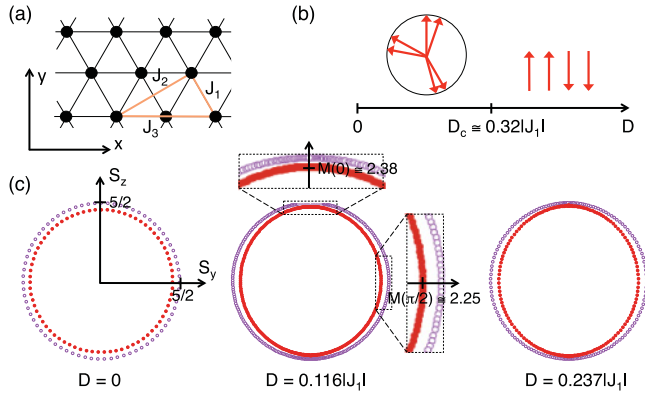
FIG. 1. (Color online) (a) The AF interactions J_1, J_2, and J_3 on a triangular-lattice AF. (b) The noncollinear state is stable when $D < D_c$. (c) The $\{S_y, S_z\}$ values for three values of the anisotropy with classical (open circles) or quantum (closed circles) spins. Regions around $\theta = 0$ and $\pi/2$ are expanded for $D/|J_1| = 0.116$.

With decreasing anisotropy [corresponding to increasing Ga doping in the compound $CuFe_{1-x}Ga_xO_2$ (Ref. [15])], the $\uparrow\uparrow\downarrow\downarrow$ phase eventually becomes unstable to a noncollinear, incommensurate phase. Assuming classical spins for the simple model described above, the critical value of the anisotropy at this first-order transition is $D_c = 0.317|J_1|$.

The $1/S$ expansion used to evaluate the effects of QFs on the spin amplitudes and angles was described in Ref. [2]. For classical spins, the wave vector Q_0 of the incommensurate spiral is plotted versus anisotropy in Fig. 2. To evaluate the effects of QFs, we employed a large unit cell of length $N/2$ in the **x** direction containing L periods of a distorted spiral with classical wave vector $Q_0 = 4\pi L/N$. Values of L and N are given by the points in Fig. 2. To describe the behavior of an incommensurate state, N should be large but not share any common factors with L.
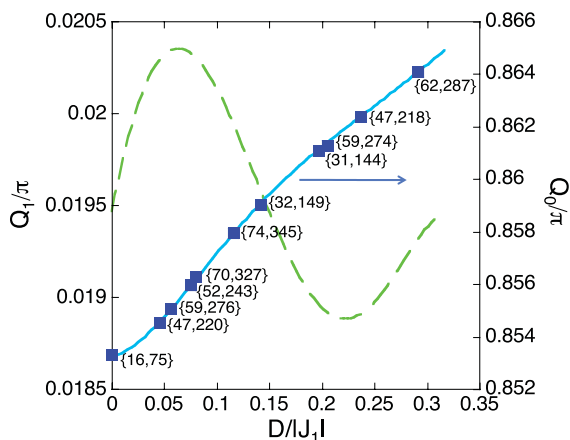

FIG. 2. (Color online) The classical wave vector Q_0 and the quantum change in wave vector Q_1 versus anisotropy. Points $\{L, N\}$ correspond to the classical wave vectors $Q_0 = 4\pi L/N$.

As discussed earlier,[11] the spin state may be expanded in odd harmonics[16] of the fundamental ordering wave vector $\mathbf{Q} = Q\mathbf{x}$:

$$\langle S_y(\mathbf{R}) \rangle = \sum_{l=0} C_y^{(2l+1)} \sin[(2l+1)Qx], \qquad (2)$$

$$\langle S_z(\mathbf{R}) \rangle = \sum_{l=0} C_z^{(2l+1)} \cos[(2l+1)Qx]. \qquad (3)$$

Hence the spiral lies in the yz plane with $C_x^{(2l+1)} = 0$. When $D = 0$, a pure spiral is recovered with $C_y^{(1)} = C_z^{(1)} = S$ and $C_\alpha^{(2l+1 \geqslant 3)} = 0$. Higher harmonics grow with increasing anisotropy as the spins favor the $\pm\mathbf{z}$ directions. For classical spins, $\sum_{l=0} C_z^{(2l+1)} = S$ because the maximum value of $\langle S_z(\mathbf{R}) \rangle$ is S.

Each odd harmonic of the spin state can be characterized by an ellipticity $p_{2l+1} = |F_y^{(2l+1)}|/|F_z^{(2l+1)}|$, where

$$F_\alpha^{(2l+1)} = \frac{1}{N} \sum_i e^{i(2l+1)\mathbf{Q}\cdot\mathbf{R}_i} \langle S_\alpha(\mathbf{R}_i) \rangle \qquad (4)$$

are the magnetic structure factors with summations restricted to the N SLs of the unit cell. Because $F_y^{(2l+1)}$ is imaginary and $F_z^{(2l+1)}$ is real, $C_y^{(2l+1)} = 2\,\mathrm{Im}(F_y^{(2l+1)})$ and $C_z^{(2l+1)} = 2\,\mathrm{Re}(F_z^{(2l+1)})$. Consequently, $p_{2l+1} = |C_y^{(2l+1)}/C_z^{(2l+1)}|$. Only the ellipticity $p_1 = |C_y^{(1)}/C_z^{(1)}|$ of the first harmonic has been of experimental interest.

Expanded about their classical values, the spin amplitudes and angles for

$$\langle \mathbf{S}(\mathbf{R}) \rangle = M(\mathbf{R})(0, \sin\theta(\mathbf{R}), \cos\theta(\mathbf{R})) \qquad (5)$$

are given by $M(\mathbf{R}) = S + M_1(\mathbf{R})$ and $\theta(\mathbf{R}) = \theta_0(\mathbf{R}) + \theta_1(\mathbf{R})/S$. Evaluating $M_1(\mathbf{R})$ requires a two-dimensional momentum integral over $|X_{rs}^{-1}|^2$, where $\underline{X}$ are the $2N \times 2N$ nonunitary matrices that diagonalize the second-order Hamiltonian H_2.[17] Evaluating $\theta_1(\mathbf{R})$ requires the inverse of the $N \times N$ Hessian $Y_{rs} = (1/N)\partial^2 E_0/\partial\theta_r\partial\theta_s$ and the N-dimensional vector $(1/N)\partial E_2/\partial\theta_r$, where E_0 is the classical energy and $E_2 = \langle H_2 \rangle$. This formalism was described in more detail in Ref. [2].

III. SPIN AMPLITUDES AND ANGLES

Results for $M_1(\mathbf{R})$ and $\theta_1(\mathbf{R})$ are most easily visualized when plotted against the classical angles $\theta_0(\mathbf{R})$ of the spins $\langle \mathbf{S}(\mathbf{R}) \rangle$. For three nonzero values of $D/|J_1|$, M_1 and θ_1 are plotted in Figs. 3(a) and 3(b). Because QFs always suppress the spin amplitude, $M_1 < 0$. Due to the D_4 symmetry of the planar magnetization $\langle \mathbf{S}(\mathbf{R}) \rangle$, $\theta_1(\theta_0)$ and $M_1(\theta_0)$ are antisymmetric and symmetric, respectively, about the points $\theta_0 = 0, \pi/2, \pi$, and $3\pi/2$.

When $D = 0$, $|M_1| = 0.216$ and $M = 2.284$ are the same at every lattice site. Since all directions are equivalent, the angular change θ_1 is not defined for $D = 0$. When $D > 0$, the Hamiltonian is no longer isotropic and, even in the classical limit, the spins favor the $\pm\mathbf{z}$ directions. The classical distortion of the spiral corresponds to a redistribution of the spin vectors around a circle. This behavior is clearly seen in Fig. 1(c) for $D/|J_1| = 0.116$, where the density of hollow points is largest
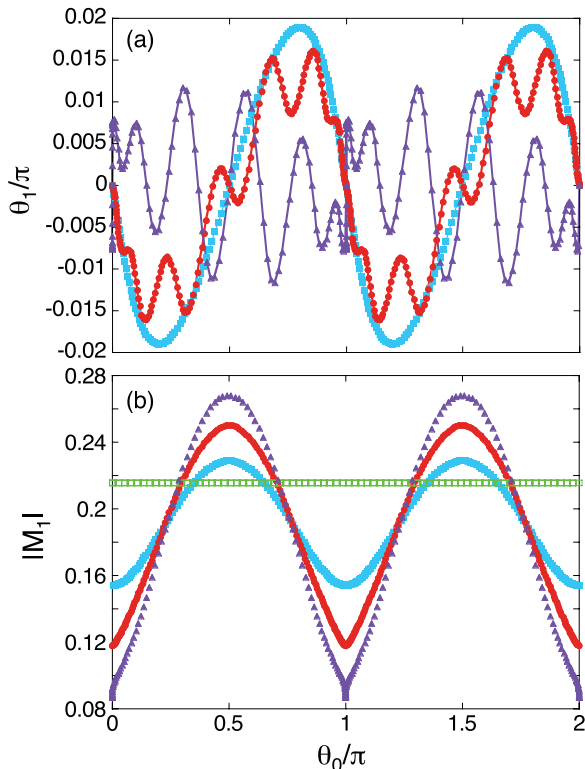
FIG. 3. (Color online) The effect of QFs on the spin (a) angles and (b) amplitudes versus θ_0/π for $D/|J_1| = 0$ (green open squares), 0.046 (blue closed squares), 0.116 (red circles), and 0.237 (purple triangles).
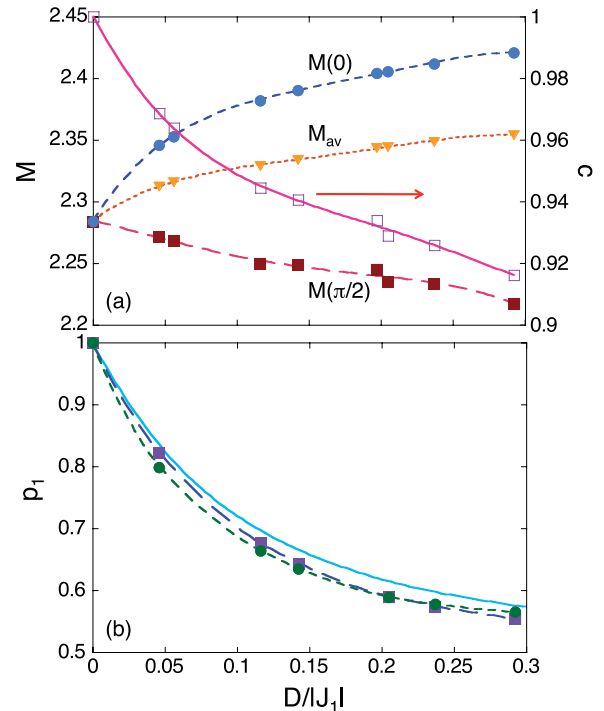

FIG. 4. (Color online) (a) The spin amplitudes parallel and perpendicular to the easy axis, $M(0)$ and $M(\pi/2)$, as well as the average spin amplitude M_{av} and the constriction $c = M(\pi/2)/M(0)$ versus anisotropy. (b) The ellipticity p_1 versus anisotropy for classical spins (solid), with QFs of the spin amplitude only (long dash and squares), and also including QFs of the angles (short dash and circles).

along the easy axis. Correspondingly, the classical ellipticity p_1 plotted in Fig. 4(b) decreases with D.

For $D = 0.046|J_1|$, Fig. 3(b) presents a nearly sinusoidal variation of $M_1(\theta_0)$ with maximum suppression along the $\theta_0 = \pi/2$ and $3\pi/2$ directions, perpendicular to the easy axis. The angular change θ_1 is negative for $0 < \theta_0 < \pi/2$ and positive for $\pi/2 < \theta_0 < \pi$. Hence θ_1 further distorts the spiral and lowers the ellipticity p_1, as shown in Fig. 4(b). For $D = 0.116|J_1|$, $|M_1|$ displays an even greater variation from the $\theta_0 = 0$ to $\pi/2$ directions and θ_1 exhibits additional oscillations with θ_0. When $D/|J_1| = 0.237$, the oscillations in θ_1 restore a more circular spiral and enhance p_1. This behavior was also found for a noncollinear 3-SL state.[2]

Separately, the changes in the spin amplitude $M_1(\theta_0)$ and the angle $\theta_1(\theta_0)$ may not have any physical significance. For example, Fig. 3(b) indicates that $|M_1(\theta_0)|$ has multiple solutions at $\theta_0 = 0$ and π when $D/|J_1| = 0.237$. However, each of these multiple solutions for $|M_1(\theta_0)|$ corresponds to a different value of $\theta_1(\theta_0)$, which also has multiple solutions at $\theta_0 = 0$ or π. The minimum suppression of the spin amplitude [corresponding to the smallest value of $|M_1|$ in Fig. 3(b)] occurs when $\theta_1 = 0$ so that the corrected spin angle $\theta = \theta_0 + \theta_1/S$ equals 0 or π.

Although the spiral becomes more distorted with increasing anisotropy, the average value of the spin amplitude $M_{av} = S - |M_1|_{av}$ is an increasing function of $D/|J_1|$, as shown in Fig. 4(a). Just above the first-order transition at D_c, $|M_1| = 0.113$ so that the amplitude of each spin in the $\uparrow\uparrow\downarrow\downarrow$ phase is $M = 2.387$. Within the collinear phase, $|M_1| \rightarrow 0$ and

$M \rightarrow 2.5$ as $D/|J_1| \rightarrow \infty$. Also plotted in Fig. 4(a) are the maximum and minimum spin amplitudes, $M(0)$ and $M(\pi/2)$, parallel and perpendicular to the anisotropy axis. Whereas $M(0)$ rises, $M(\pi/2)$ falls with increasing $D/|J_1|$.

The turn angles of the spiral are also affected by QFs. For a pure spiral with $D = 0$, the turn angle $\phi = \theta(\mathbf{R} + \mathbf{x}/2) - \theta(\mathbf{R}) = Q/2$ is the same everywhere along the spiral. For $D > 0$, the distribution of turn angles around $Q/2$ causes the spins to favor the anisotropy axis.[15] With $D/|J_1| = 0.116$, histograms of the turn angles for classical and quantum spirals with $S = 5/2$ are plotted in Fig. 5. Notice that QFs broaden the distribution of turn angles for the distorted spiral.

IV. SPIRAL PARAMETERS

QFs significantly alter the harmonic structure of the distorted spiral. For $D = 0.237|J_1|$, the classical and quantum spin states are characterized by the parameters given in Table I. While only slightly reducing $p_1 = |C_y^{(1)}/C_z^{(1)}|$ from 0.599 to 0.578 and leaving $p_3 = |C_y^{(3)}/C_z^{(3)}| \approx 1.37$ almost unchanged, QFs suppress the harmonic ratios $|C_z^{(3)}/C_z^{(1)}|$ and $|C_z^{(5)}/C_z^{(1)}|$ by 9% and 35%, respectively. Quantum effects also expand the harmonic range of the spin state: the classical spiral has no significant harmonics above seventh order but the quantum spiral has significant ninth-order harmonics.
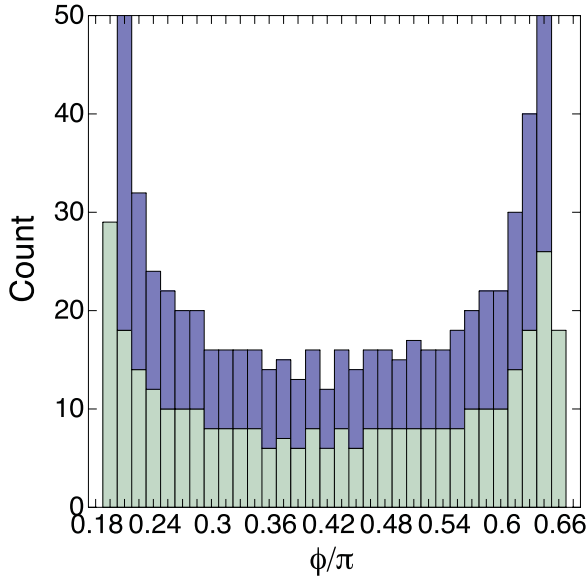
FIG. 5. (Color online) Histogram of the turn angles ϕ for a classical (dark or blue) or quantum (light or green) spiral with $D/|J_1| = 0.116$.

The effect of QFs on the wave vector $Q = Q_0 + Q_1/S$ of the incommensurate spiral is obtained by minimizing $E(Q) = E(Q_0 + Q_1/S)$ with respect to Q_1. Results for

$$Q_1 = -\frac{\partial E_2/\partial Q|_{Q_0}}{\partial^2 E_0/\partial Q^2|_{Q_0}} \qquad (6)$$

are plotted in Fig. 2. Since $Q_1 > 0$, QFs enhance the incommensurate wave vector, nudging it closer to the wave vector $Q_{4\text{-}SL} = \pi$ of the nearby $\uparrow\uparrow\downarrow\downarrow$ phase. For $S = 5/2$, Q_1 raises the wave vector of the incommensurate spiral by about 1%.

The change in critical anisotropy $D_c = D_0 + D_1/S$, above which the $\uparrow\uparrow\downarrow\downarrow$ phase is stable, can be evaluated by setting the energy $E(Q_0 + Q_1/S, D_0 + D_1/S)$ to be the same above and below the first-order transition. This yields the expression

$$D_1 = -\frac{E_2(Q_0, D_0^-) - E_2(Q_{4\text{-}SL}, D_0^+)}{\partial E_0/\partial D|_{Q_0, D_0^-} - \partial E_0/\partial D|_{Q_{4\text{-}SL}, D_0^+}}. \qquad (7)$$

We find that $D_1 = 0.602 \times 10^{-2}|J_1|$, corresponding to a 0.8% increase in the critical anisotropy from $D_c = 0.317|J_1|$ for classical spins to $0.319|J_1|$ for $S = 5/2$.

As indicated by Fig. 4(b), the quantum corrections to the ellipticity p_1 are rather modest and cannot be easily separated from the classical ellipticity. For $S = 5/2$, the maximum reduction of the ellipticity by QFs is about 4%. However, the effects of QFs can be experimentally distinguished from the classical distortion by measuring the *constriction* of the spiral, defined as $c = M(\pi/2)/M(0)$. The constriction is plotted

versus anisotropy in Fig. 4(a). Comparing Figs. 4(a) and 4(b) reveals that c is always much closer to 1 than p_1. Since $c \approx 1 - (|M_1(\pi/2)| - |M_1(0)|)/S$, the reduction of c from 1 must be attributed entirely to QFs.

In terms of the harmonic coefficients, the spin amplitudes perpendicular and parallel to the anisotropy axis are given by $M(\pi/2) = \sum_{l=0}(-1)^l C_y^{(2l+1)}$ and $M(0) = \sum_{l=0} C_z^{(2l+1)}$. Hence $c = \sum_{l=0}(-1)^l C_y^{(2l+1)}/\sum_{l=0} C_z^{(2l+1)}$. Although elastic neutron-scattering measurements provide only the absolute values $|C_\alpha^{(2l+1)}|$, the fact that $C_\alpha^{(1)} > 0$ and $C_\alpha^{(3)} < 0$ can be used to estimate

$$c \approx \frac{|C_y^{(1)}| + |C_y^{(3)}|}{|C_z^{(1)}| - |C_z^{(3)}|} = p_1 \frac{1 + |C_y^{(3)}/C_y^{(1)}|}{1 - |C_z^{(3)}/C_z^{(1)}|}, \qquad (8)$$

which assumes that $|C_\alpha^{(2l+1 \geqslant 5)}/C_\alpha^{(1)}| \ll 1$. Notice that $c = p_1$ only when the third and higher harmonics are absent. For $D/|J_1| = 0.116$, this approximation yields $c \approx 0.951$, slightly larger than the exact result of 0.945.

V. CONCLUSION

Based on Fig. 4(b), an anisotropy of $D/|J_1| = 0.025$ corresponds to the measured ellipticity $p_1 \approx 0.9$ of doped $CuFeO_2$.[10] Since the two-dimensional results of this paper may slightly overestimate QFs compared to the results of a (much more demanding) three-dimensional calculation, we conclude that the effect of anisotropy on a classical spiral explains most observed properties of $CuFeO_2$. The small value of $D/|J_1|$ qualitatively agrees with recent fits[15] of D and J_1 based on the excitation spectrum of doped $CuFeO_2$, which indicate that $D/|J_1|$ lies between 0.026 and 0.079. With $D/|J_1| = 0.025$, the constriction of the spiral in $CuFeO_2$ would be $c \approx 0.98$, very close to the classical limit of 1.

To summarize, QFs have highly nontrivial effects on the spiral state of a geometrically frustrated triangular-lattice AF with easy axis anisotropy. Although the average spin amplitude rises with the anisotropy, the spiral also becomes more distorted. Angular changes act to further distort the spin state for small anisotropy but to reduce the distortion for strong anisotropy. While QFs enhance the wave vector of the incommensurate state, they also favor the spiral over the neighboring $\uparrow\uparrow\downarrow\downarrow$ state.

Suitably generalized to include additional harmonics produced by lattice distortions within the hexagonal planes,[15] we hope that the results of this paper can be used to estimate the constriction c for multiferroic $CuFeO_2$ and other materials[5–7] that exhibit incommensurate spiral order.

TABLE I. Structure of the spiral for $D = 0.237|J_1|$.

	$C_y^{(1)}$	$C_y^{(3)}$	$C_y^{(5)}$	$C_z^{(1)}$	$C_z^{(3)}$	$C_z^{(5)}$	p_1
Classical	1.762	−0.695	0.037	2.937	−0.505	0.066	0.599
Quantum	1.619	−0.601	0.020	2.805	−0.439	0.041	0.578

[1] See, for example, K. Yosida, *Theory of Magnetism* (Springer, Berlin, 1996), Chap. 9.

[2] R. S. Fishman, Phys. Rev. B **84**, 052405 (2011).

[3] M. Poienar, F. Damay, C. Martin, V. Hardy, A. Maignan, and G. André, Phys. Rev. B **79**, 014412 (2009).

[4] E. Rastelli and A. Tassi, J. Appl. Phys. **73**, 6995 (1993); R. Darradi, J. Richter, and D. J. J. Farnell, Phys. Rev. B **72**, 104425 (2005); H. Katsura, S. Onoda, J. H. Han, and N. Nagaosa, Phys. Rev. Lett. **101**, 187207 (2008); J. Reuther and R. Thomale, Phys. Rev. B **83**, 024402 (2011).

[5] H. R. Child, W. C. Koehler, E. O. Wollan, and J. W. Cable, Phys. Rev. **138**, A1655 (1965); C. F. Majkrzak, J. Kwo, M. Hong, Y. Yafet, D. Gibbs, C. L. Chien, and J. Bohr, Adv. Phys. **40**, 99 (1991).

[6] M. Kenzelmann, A. B. Harris, S. Jonas, C. Broholm, J. Schefer, S. B. Kim, C. L. Zhang, S.-W. Cheong, O. P. Vajk, and J. W. Lynn, Phys. Rev. Lett. **95**, 087206 (2005); T. Arima, A. Tokunaga, T. Goto, H. Kimura, Y. Noda, and Y. Tokura, *ibid.* **96**, 097202 (2006); N. Lee, Y. J. Choi, M. Ramazanoglu, W. Ratcliff, V. Kiryukhin, and S. W. Cheong, Phys. Rev. B **84**, 020101(R) (2011).

[7] G. Lautenschläger, H. Weitzel, T. Vogt, R. Hock, A. Böhm, M. Bonnet, and H. Fuess, Phys. Rev. B **48**, 6087 (1993); G. Lawes, A. B. Harris, T. Kimura, N. Rogado, R. J. Cava, A. Aharony, O. Entin-Wohlman, T. Yildrim, M. Kenzelmann, C. Broholm, and A. P. Ramirez, Phys. Rev. Lett. **95**, 087205 (2005); D. Lebeugle, D. Colson, A. Forget, and M. Viret, Appl. Phys. Lett. **91**, 022907 (2007); Y. J. Choi, J. Okamoto, D. J. Huang, K. S. Chao, H. J. Lin, C. T. Chen, M. van Veenendaal, T. A. Kaplan, and S.-W. Cheong, Phys. Rev. Lett. **102**, 067601 (2009).

[8] S. Seki, Y. Yamasaki, Y. Shiomi, S. Iguchi, Y. Onose, and Y. Tokura, Phys. Rev. B **75**, 100403(R) (2007); S. Kanetsuki, S. Mitsuda, T. Nakajima, D. Anazawa, H. A. Katori, and K. Prokes, J. Phys.: Condens. Matter **19**, 145244 (2007).

[9] D. I. Khomskii, J. Magn. Magn. Mater. **306**, 1 (2006); S.-W. Cheong and M. Mostovoy, Nat. Mater. **6**, 13 (2007); Y. Tokura and S. Seki, Adv. Mater. **22**, 1554 (2010).

[10] T. Nakajima, S. Mitsuda, K. Takahashi, M. Yamano, K. Masuda, H. Yamazaki, K. Prokes, K. Kiefer, S. Gerischer, N. Terada, H. Kitazawa, M. Matsuda, K. Kakurai, H. Kimura, Y. Noda, M. Soda, M. Matsuura, and K. Hirota, Phys. Rev. B **79**, 214423 (2009).

[11] R. S. Fishman and S. Okamoto, Phys. Rev. B **81**, 020402 (2010).

[12] R. S. Fishman, Phys. Rev. Lett. **106**, 037206 (2011).

[13] F. Ye, J. A. Fernandez-Baca, R. S. Fishman, Y. Ren, H. J. Kang, Y. Qiu, and T. Kimura, Phys. Rev. Lett. **99**, 157201 (2007); R. S. Fishman, F. Ye, J. A. Fernandez-Baca, J. T. Haraldsen, and T. Kimura, Phys. Rev. B **78**, 140407(R) (2008).

[14] S. Mitsuda, H. Yoshizawa, N. Yaguchi, and M. Mekata, J. Phys. Soc. Jpn. **60**, 1885 (1991).

[15] J. T. Haraldsen, F. Ye, R. S. Fishman, J. A. Fernandez-Baca, Y. Yamaguchi, K. Kimura, and T. Kimura, Phys. Rev. B **82**, 020404 (2010).

[16] M. E. Zhitomirsky and I. A. Zaliznyak, Phys. Rev. B **53**, 3428 (1996).

[17] The Hamiltonian and energy are expanded in powers of $1/\sqrt{S}$. The first-order $1/\sqrt{S}$ term $E_1 = \langle H_1 \rangle$ vanishes but the second-order $1/S$ term $E_2 = \langle H_2 \rangle$ is nonzero. Note that $J_n S^2$ and $D S^2$ are considered of order 1.